Editors' Suggestion

Statistical mechanics of multiplectoneme phases in DNA

Midas Segers [1,*] Enrico Skoruppa [2,*] Helmut Schiessel [2,3] and Enrico Carlon [1]
[1]*Soft Matter and Biophysics, KU Leuven, Celestijnenlaan 200D, 3001 Leuven, Belgium*
[2]*Cluster of Excellence Physics of Life, TU Dresden, 01062 Dresden, Germany*
[3]*Institut für Theoretische Physik, TU Dresden, 01062 Dresden, Germany*

(Received 31 October 2024; accepted 6 March 2025; published 17 April 2025)

A stretched DNA molecule that is also under- or overwound undergoes a buckling transition, forming intertwined looped domains called plectonemes. Here we develop a simple theory that extends the two-phase model of stretched supercoiled DNA, allowing for the coexistence of multiple plectonemic domains by including positional and length distribution entropies. Such a multiplectoneme phase is favored in long DNA molecules in which the gain of positional entropy compensates for the cost of nucleating a plectoneme along a stretched DNA segment. Despite its simplicity, the developed theory is shown to be in excellent agreement with Monte Carlo simulations of the twistable wormlike chain model. The theory predicts more plectonemes than experimentally observed, which we attribute to the limited resolution of experimental data. Since plectonemes are detected through fluorescence signals, those shorter than the observable threshold are likely missed.

DOI: 10.1103/PhysRevE.111.044408

I. INTRODUCTION

In the cellular environment, DNA typically exists in a torsionally underwound state, a conformation finely regulated by the concerted activity of enzymes such as topoisomerases and polymerases [1]. Over- and underwound DNAs—also called supercoiled DNA—exhibit a distinct response to the imposed torsional strain that culminates in the assumption of superhelically coiled configurations called plectonemes [2,3] (from the Greek *pléko*, braid, and *níma*, filament; see Fig. 1). The transition into the plectonemic state is commonly referred to as DNA buckling. Supercoiling is important for a multitude of biological processes, such as the regulation of gene expression [4–7], the maintenance of chromatin architecture [8–13], and retroviral integration [14]. One mechanism by which supercoiling promotes biological function is the induction of proximity between distal sites to favor, for example, the binding of DNA-bridging proteins [14–18] and the interaction between promoter-enhancer pairs [19,20]. The broad phenomenology of DNA supercoiling has been studied extensively due to its relevance in biology [18,21–34], yet many aspects remain elusive. Whether supercoiling is a plausible mechanism leveraged in the establishment of DNA bridges critically depends on the relation between the distance of the binding motives and the typical size of plectonemes. If the distance between these sites significantly exceeds the characteristic size of a plectoneme, supercoiling is unlikely to contribute to the establishment of proximity between the relevant segments. Conversely, binding between motives within the range of characteristic plectoneme lengths is likely enhanced by supercoiling. In this work, we explore to which degree supercoiling is segregated into multiple plectonemes and how this distribution is influenced by external forces and torques.

We study this phenomenology in the context of single-molecule magnetic tweezers (MTs) [35–37], which have emerged as prominent tools for the experimental exploration of DNA supercoiling. In MT experiments, a single DNA molecule is tethered between a superparamagnetic bead and a flowcell surface. Exposure of the bead to an appropriately calibrated magnetic field allows for the induction of linear stretching forces (see Fig. 1). Additionally, rotating the field-inducing magnet enables the torsional state of the molecule to be controlled. This torsional state corresponds to the mutual wrapping of the two individual strands of a double-stranded DNA molecule. In the torsionally relaxed state, these strands wrap around each other approximately once every 10.5 base pairs, resulting in a relaxed state linking approximately $\mathrm{Lk}_0 \approx N/10.5$ for a molecule consisting of N base pairs. Rotation of the bead induces an excess linking strain $\Delta\mathrm{Lk}{=}\mathrm{Lk} - \mathrm{Lk}_0{\neq}0$.

The classical readout of these experiments is limited to the tether extension (i.e., the bead-surface distance), which may be observed in terms of the number of turns imposed on the bead. Plectoneme formation becomes indirectly visible due to the significant and progressive reduction in tether extension with increasing linking strain. This behavior—characterized by the mean extension [3,24,36–40] and extension fluctuations [18,32]—is well understood. However, this readout does not yield access to the morphology and phase characteristics of the underlying molecule. Several studies have attempted to shed light on these characteristics by combining MT (or similar) setups with fluorescent microscopy, which enables the visualization of the molecule [25,41]. Van Loenhout *et al.* [25] demonstrated the propensity of DNA to nucleate into more than one plectoneme. In the present work, we revisit this observation by leveraging a combination of simulation and analytical approaches.

In theoretical treatments of DNA supercoiling, introducing the supercoiling density $\sigma = \Delta\mathrm{Lk}/\mathrm{Lk}_0$ proves convenient because it is independent of the molecule's curvilinear length.

*These authors contributed equally to this work.

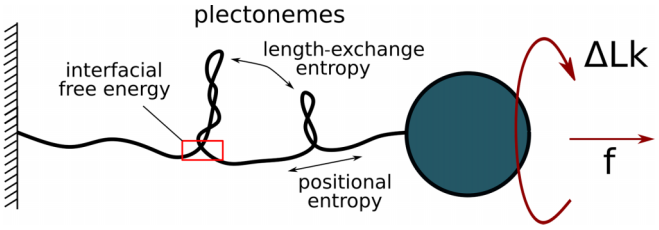

FIG. 1. Setup of a typical DNA magnetic tweezers experiment. The DNA molecule is tethered at one end to a solid surface and at the other to a paramagnetic bead. A magnetic field is applied which exerts a linear force f and rotates the bead to a ΔLk number of turns (counted with respect to the torsionally relaxed state). When ΔLk exceeds a threshold value, the molecule buckles, and plectonemic supercoils appear. We develop a theory of multiplectonemes that incorporates a free-energy penalty for plectoneme nucleation along with two entropic terms: one for positional entropy and another for length-exchange entropy.

Due to its chiral nature, DNA exhibits a different response to overwinding ($\sigma > 0$) versus underwinding ($\sigma < 0$). Notably, underwinding, coupled with adequate stretching forces, leads to a structural transition known as torsionally induced melting [42]. However, this transition predominantly occurs for stretching forces exceeding 1 pN [21]. Here, we restrict our analysis to the linear elastic regime, ignoring higher-order transitions, thus rendering our approach fully symmetric regarding over- and underwinding.

DNA buckling is commonly described as a (pseudo) first-order phase transition [39]. While gradually increasing σ starting from the torsionally relaxed state ($\sigma = 0$), the tethered molecule initially remains in an elongated state until a threshold value $\sigma = \sigma_s$ is reached. Beyond this (buckling) point, plectonemes nucleate along the stretched phase, as depicted in Fig. 1. This transition comes at the cost of a considerable reduction in tether extension but enables the absorption of more linking strain due to the crossings within the plectonemes, i.e., the supercoiling density of plectonemes exceeds that of the stretched phase ($\sigma_p > \sigma_s$). This phenomenon resembles liquid-vapor coexistence, where the two phases are maintained at different particle densities ($n_{\rm liq} > n_{\rm vap}$).

In this work, we employ efficient Monte Carlo simulations (MC) of a discrete twistable wormlike chain (TWLC) to infer the physical properties of plectonemes in stretched and torsionally constrained DNA. Moreover, we develop a simple statistical mechanical approach that describes a DNA molecule as a chain consisting of stretched and plectonemic phase segments. The model features a free energy penalty associated with the interface between the two phases that tends to suppress plectoneme nucleation. Nevertheless, in long DNA molecules, the nucleation of multiple plectonemes becomes entropically favorable. We account for two types of entropic contributions: positional entropy, which reflects the number of possible positions for plectonemes along the stretched segments, and length-exchange entropy, which describes the partitioning of the total plectonemic length among different plectonemes (see Fig. 1), similar to Ref. [43]. Throughout this work, we refer to this model as the multiplectoneme model (MP).

Our approach of accounting for the positioning and length distribution entropy is very similar to those employed in prior studies [43,44]. These works developed sophisticated geometric descriptions for the plectoneme free energy accounting for a host of different factors, including the twist and bending strains within the superhelical winding, electrostatic interactions, confinement entropy, plectoneme tail bending, and end loop contributions. Due to their complexity, these approaches require extensive numerical optimization and are subject to various approximations. To avoid these complications, we employ a much simpler empirical free energy that was derived via umbrella sampling of MC simulations in previous work [32]. Despite its simplicity, the model displays excellent agreement with MC-generated data regarding the average number of plectonemes, their lengths, and distribution, as well as other quantities such as the torque versus supercoiling density. Moreover, we demonstrate the model to reproduce additional features observed in a recent MT study [45].

This paper is organized as follows: Section II reviews the two-phase model of stretched DNA buckling and introduces the theoretical framework of the multiplectoneme model. Section III introduces the Monte Carlo simulations and the methodology of inference for the relevant observables. The simulation readout is then compared to the model predictions for various quantities. Contextualization and comparison with experimental data are provided in Sec. IV. Finally, Sec. V concludes the paper by highlighting the relevance of our findings.

II. MODELING THE MULTIPLECTONEME STATE

In the two-phase model of stretched DNA buckling, a DNA molecule of length L subject to a stretching force f and at fixed supercoil density σ is described as consisting of two distinct phases [3,39]: the stretched phase and plectonemic phases, with corresponding free energies per unit length $\mathcal{S}(\phi)$ and $\mathcal{P}(\psi)$, respectively, where ϕ and ψ are the supercoil densities in the two phases.

For the introduction of the theoretical description, we restrict the discussion to simple quadratic free energies that allow for closed-form expressions for many relevant quantities and therefore serve for illustration. When comparing to Monte Carlo-sampled and experimental data, we incorporate higher-order corrections that have been shown in previous work to provide superior agreement with MT and MC data [32] (see Appendix A). In this quadratic description, the free energies of the two phases are given by [39]

$$\mathcal{S}(\phi) = -g(f) + a(f)\phi^2, \tag{1}$$

$$\mathcal{P}(\psi) = b\psi^2. \tag{2}$$

The free energy of the stretched phase, Eq. (1), can be derived from the twistable wormlike chain (TWLC) as a high-force expansion [38,46]. The theory yields the coefficients

$$g(f) = f\left(1 - \sqrt{\frac{k_B T}{Af}} + \cdots\right), \tag{3}$$

$$a(f) = \frac{C}{2}\left(1 - \frac{C}{4A}\sqrt{\frac{k_B T}{Af}} + \cdots\right) k_B T \omega_0^2, \tag{4}$$

where A is the bending stiffness, C is the twist stiffness, and ω_0 is the intrinsic twist of the double helix. Throughout this work, we use the values $A = 40$ nm, $C = 100$ nm, which were shown to yield excellent agreement with MT data [18], and $\omega_0 = 1.75$ nm^{-1}. The high-force expansions (3), and (4) are valid in the regime $k_BT/Af \ll 1$, which corresponds roughly to $f > 0.5$ pN. The plectonemic free energy (2) is phenomenological and may be viewed as a lowest-order expansion of the underlying free energy. The parameter b is usually expressed as

$$b = \tfrac{1}{2} P k_B T \omega_0^2, \tag{5}$$

where P is referred to as the effective torsional stiffness of the plectonemic phase [45], which by analogy to A and C is expressed in units of length. Assuming a fraction ν of the molecular length to be contained in the stretched phase—and consequently a fraction $(1-\nu)$ in the plectonemic phase—the total free energy can be written as [39]

$$\mathcal{F}(\phi, \psi, \nu) = \nu \mathcal{S}(\phi) + (1-\nu)\mathcal{P}(\psi). \tag{6}$$

Minimization of $\mathcal{F}$ under the constraint of fixed total linking number—or equivalently total supercoiling density $\sigma = \nu\phi + (1-\nu)\psi$—leads to a double tangent construction [39].

In terms of the parameters of the free energies, one finds the phase boundaries [32]

$$\sigma_s = \sqrt{\frac{b\,g}{a(a-b)}}, \quad \sigma_p = \sqrt{\frac{a\,g}{b(a-b)}}, \tag{7}$$

which mark the limits of the regime of coexisting plectoneme and stretched phases: $\sigma_s < |\sigma| < \sigma_p$. At supercoiling densities smaller than σ_s ($|\sigma| < \sigma_s$), the molecule is in a pure stretched phase, referred to as the pre-buckling regime. Conversely, supercoiling densities exceeding σ_p ($|\sigma| > \sigma_p$) mark a pure plectonemic phase. Partial or fully plectonemic states are commonly referred to as the post-buckling regime. This simple theory describes buckling as a thermodynamic first-order transition. Note that this description does not account for the distribution of the two phases (corresponding to more than one plectoneme) along the molecule.

A. The torque ensemble

Entropically, the nucleation of multiple plectonemes is favored over the formation of a single plectonemic domain. However, the propensity for local phase-switches is constrained by free-energy penalties associated with the cost of generating plectoneme end-loops and tails. Consequently, the average number of plectonemes is determined by the interplay between the entropic gain and enthalpic loss associated with plectoneme nucleation. These effects cannot be accounted for by the two-phase theory introduced above since it only considers the balance between the two phases and not their distribution along the chain. For the incorporation of the occurrence of multiple plectonemes in the thermodynamic description, it turns out to be advantageous to consider the fixed torque ensemble ($\tau = \text{cte}$) instead of the fixed linking number ensemble ($\sigma = \text{cte}$). Although this ensemble differs from the scenarios typically considered experimentally, we are still able to deduce key observables relevant to the linking

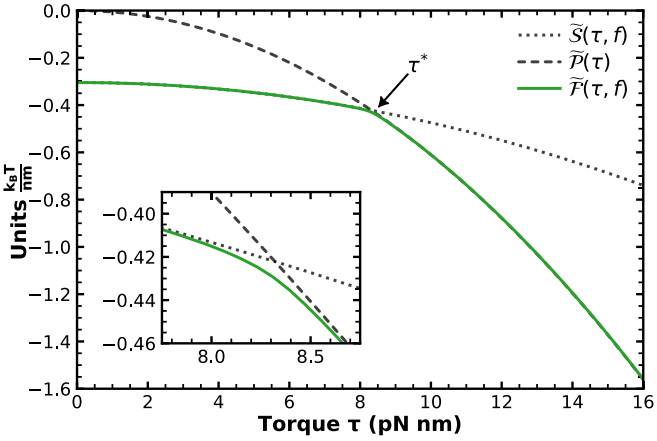

FIG. 2. Free-energy densities in the torque ensemble. Dashed and dotted lines: free energies of the stretched (9) and plectonemic (10) phases, respectively. Green solid line: Free energy per unit length of the MP model, from Eq. (22), vs torque. The inset provides a close-up view of the free energies near the buckling torque, highlighting the smooth transition captured by the MP model. The parameters used for the graphs are $f = 0.5$ pN, $\mu = 50$ pN nm, and $l_c = 100$ nm. The corresponding buckling torque [from Eq. (11)] is $\tau^* = 8.32$ pN nm.

number ensemble. In the context of MT experiments, torque is related to the free energy via a partial derivative with respect to θ, the rotation angle described by the bead, which is proportional to the supercoiling density $\theta = L\omega_0\sigma$,

$$\tau = \frac{1}{\omega_0}\frac{\partial \mathcal{F}}{\partial \sigma}, \tag{8}$$

where $\mathcal{F}$ is the free energy per unit length. Stretched- and plectonemic-phase free energies in the torque ensemble are related to the linking number analogous via Legendre transforms. Transformation of Eqs. (1) and (2) yields

$$\widetilde{\mathcal{S}}(\tau) = -g - \frac{\omega_0^2}{4a}\tau^2, \tag{9}$$

$$\widetilde{\mathcal{P}}(\tau) = -\frac{\omega_0^2}{4b}\tau^2. \tag{10}$$

In the torque ensemble, the buckling torque is obtained from the condition $\widetilde{\mathcal{S}}(\tau^*) = \widetilde{\mathcal{P}}(\tau^*)$ which gives

$$\tau^* = \frac{2}{\omega_0}\sqrt{\frac{abg}{a-b}}. \tag{11}$$

The condition of equal torque implies the total free energy to be given by the minimum of the two individual contributions,

$$\widetilde{\mathcal{F}}(\tau) = \min_{\tau}(\widetilde{\mathcal{S}}(\tau), \widetilde{\mathcal{P}}(\tau)). \tag{12}$$

which is valid in the thermodynamic limit $L \to \infty$. This means that, in this approximation, the molecule remains fully in the stretched state for $|\tau| \leqslant \tau^*$ [$\widetilde{\mathcal{F}}(\tau) = \widetilde{\mathcal{S}}(\tau)$] and then immediately transitions into the fully plectonemic state for $|\tau| \geqslant \tau^*$ [$\widetilde{\mathcal{F}}(\tau) = \widetilde{\mathcal{P}}(\tau)$]. The dotted and dashed lines in Fig. 2 are plots of the stretched and plectonemic phase free energies for the quadratic model. The intersection between these two curves corresponds to the buckling torque τ^*.

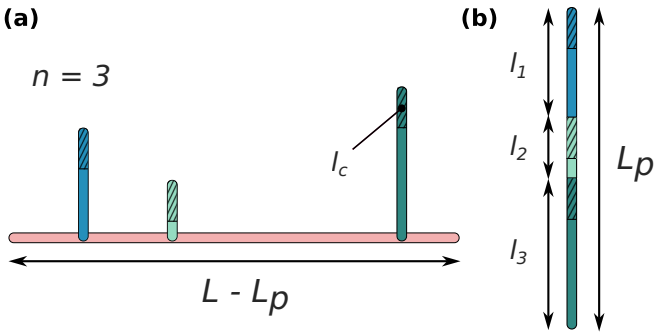

FIG. 3. Schematic representation of the MP model for a multiplectonemic phase with $n = 3$ plectonemes. (a) The configurational entropy (14) quantifies the number of possible ways to distribute n plectonemes along a stretched segment of length $L - L_p$. (b) The number of ways the cumulative plectoneme length L_p can be partitioned over the given number of plectonemes gives rise to the length-exchange entropy (16). The hatched regions indicate the minimal size of the plectoneme l_c in the MP model.

B. The multiplectoneme model

We use the two-phase description of DNA supercoiling to obtain the free energy associated with the multiplectonemic phase. We distinguish between three separate contributions to the multiplectonemic phase free energy: one enthalpic and two entopic components. Assuming a multiplectonemic phase of n plectonemes with a cumulative length L_p, the enthalpic contribution to the free energy is given by

$$F_{\text{enth.}}(L, L_p, n) = (L - L_p)\widetilde{\mathcal{S}} + L_p\widetilde{\mathcal{P}} + n\mu, \tag{13}$$

where $\mu > 0$ is the free energy cost of inserting a plectoneme within a stretched-phase domain. This may be viewed as an effective elastic term for the necessary bending to transition into a plectoneme and the creation of a plectoneme end-loop.

A large value of μ results in a propensity towards the formation of relatively few, but larger plectonemic domains, whereas small values of μ favor the formation of a relatively large amount of short plectonemes. The nucleation free energy μ serves as a free parameter in our theory and will be fitted to Monte Carlo data, as discussed in detail in Sec. III.

The remaining entropic contributions to the free energy have been derived previously in Ref. [43]. The first component is the positional entropy. It counts the number of configurations in which the n plectonemes can be inserted along the stretched phase (of length $L - L_p$),

$$\Omega_n(L_p) = \frac{1}{n!}\left(\frac{L - L_p}{\Delta l}\right)^n, \tag{14}$$

as illustrated in Fig. 3(a). To make $\Omega_n(L_p)$ dimensionless, we introduced a discretization length Δl, which rescales all lengths. Technically, this introduces configurations for which plectonemes occupy the same site. However, for sufficiently small values of Δl, the statistical weight of such configurations becomes vanishingly small. Note that this expression is exact in the continuum limit. In practice, we choose a discretization length of 1 nm. The second entropic component originates from partitioning the cumulative plectonemic length L_p among n different plectonemes. To discriminate small and nonphysical plectonemic domains, we introduce a length cutoff l_c, which constitutes the minimal size of a plectoneme. The partitioning of a segment of total length L_p into n segments of minimal length l_c consists in splitting the interval $[0, L_p]$ into subintervals of lengths $l_1, l_2, \ldots, l_n$ with $\sum_k l_k = L_p$ and fulfilling the constraints

$$l_c \leqslant l_k \leqslant L_p - (n - k)l_c - \sum_{m=1}^{k-1} l_m. \tag{15}$$

The number of ways in which this partitioning can be done is given by

$$\Lambda_n(L_p) = \frac{1}{(n-1)!}\left(\frac{L_p - nl_c}{\Delta l}\right)^{n-1}, \tag{16}$$

which corresponds to the partition function of a hard rod model.

Combining enthalpic (13) and entropic (14), (16) terms and summing up all possible lengths of the plectonemic phase L_p (at fixed torque τ), we obtain the total partition function for n plectonemes

$$Z(n) = \sum_{L_p} e^{-\beta F_{\text{enth.}}(L, L_p, n)}\Omega_n(L_p)\Lambda_n(L_p), \tag{17}$$

with $\beta = 1/k_BT$ and where the sum runs over values of L_p which are multiples of the discretization length Δl and with $nl_c \leqslant L_p \leqslant L$. Using the change of variable $x \equiv (L_p - nl_c)/(L - nl_c)$ we can recast (17) in the following continuum integral form:

$$Z(n) = \frac{\alpha_n}{n!(n-1)!}\int_0^1 e^{-\gamma_n x}(1 - x)^n x^{n-1} dx, \tag{18}$$

where

$$\alpha_n \equiv e^{-\beta F_{\text{enth.}}(L, nl_c, n)}\left(\frac{L - nl_c}{\Delta l}\right)^{2n}, \tag{19}$$

and

$$\gamma_n \equiv \beta(L - nl_c)(\widetilde{\mathcal{P}} - \widetilde{\mathcal{S}}). \tag{20}$$

Note that γ_n is positive for $\tau < \tau^*$ and negative for $\tau > \tau^*$.

The total partition function of a DNA molecule of length L is obtained by summing over the number of plectonemes n

$$Z_{\text{TOT}}(L) = \sum_{n=0}^{n_{\max}} Z(n), \tag{21}$$

where the maximum number of plectonemes is set $n_{\max}l_c = L$. For the range of lengths considered in this work—$L \approx 10$ μm corresponding to ≈30 kb—the sum in (21) can be safely truncated to $n \leqslant 20$ because the statistical weight of configurations with larger numbers of plectonemes is negligible. The free energy per unit length is then given by

$$\widetilde{\mathcal{F}} = -\frac{k_BT}{L}\log Z_{\text{TOT}}(L). \tag{22}$$

In practice, we calculate Z_{TOT} by approximating (18) via Laplace's method and evaluating the summation in (21) numerically. The solid green line of Fig. 2 is a plot of $\widetilde{\mathcal{F}}$ vs the torque τ for the MP model. This free energy closely matches the stretched and plectonemic free energy sufficiently far from

the transition region $\tau = \tau^*$ but it exhibits a smooth transition rather than the sharp crossing predicted by the two-phase model.

To relate measurements carried out in the fixed linking number ensemble to predictions from our theoretical model calculated within the fixed torque ensemble, we note that the first moments in the two ensembles are equivalent. One can calculate the mean supercoiling density by differentiation of the free-energy density,

$$\langle \sigma \rangle = -\frac{1}{\omega_0}\frac{\partial \widetilde{\mathcal{F}}}{\partial \tau}. \tag{23}$$

The central observables of interest in this work are the mean number of plectonemes $\langle n \rangle$ and the plectoneme length distribution $P_{\mathrm{pl}}(l)$. The former is given by

$$\langle n \rangle = \frac{\sum_n nZ(n)}{Z_{\mathrm{TOT}}}, \tag{24}$$

while the latter is found as the relative weight of those configurations containing at least one plectoneme of length l. For this, we calculate the subensemble partition function $Z(n, l)$, for states containing n plectonemes of which one has fixed length l. Note that this does not affect the enthalpic term (13) nor the positional entropy (14). However, for this subensemble the length partitioning entropy is now given by

$$\Lambda_n^*(L_p, l) = \frac{n}{(n-2)!}\left(\frac{L_p - (n-1)l_c - l}{\Delta l}\right)^{n-2}. \tag{25}$$

This is analogous to Eq. (16) because it describes the different ways one can partition the free length $L_p - l$ among $n-1$ plectonemes. Furthermore, we included a factor n because any of the n plectonemes is allowed to have length l. Hence the partition function is found to be

$$Z(n, l) = \sum_{L_p} e^{-\beta F_{\mathrm{enth.}}(L, L_p, n)}\Omega_n(L_p)\Lambda_n^*(L_p, l), \tag{26}$$

where the sums runs over multiples of Δl for $(n-1)l_c + l \leqslant L_p \leqslant L$. Finally, the probability of having a configuration in which at least one of the plectonemes has length l is

$$P_{\mathrm{pl}}(l) = \frac{1}{\sum_{n=1}^{n_{\max}}\sum_{l=l_c}^{L-nl_c} Z(n, l)}\sum_{n=1}^{n_{\max}} Z(n, l) \tag{27}$$

The theory developed here differs from prior approaches [43,44] by replacing the geometric description of the plectoneme state with a phenomenological plectoneme free energy $\widetilde{\mathcal{P}}$, fitted from independent umbrella sampling simulations [32], which allows us to cast the description in a much-simplified form. The difference between our $\widetilde{\mathcal{P}}$ and the free energy according to the theory of Marko and Neukirch [44] is discussed in some detail in Appendix B.

An alternative theoretical approach, based on a transfer matrix (TM) calculation, is described in Appendix C. While the TM and MP models show good agreement for several physical quantities, they are individually subject to distinct limitations. In the TM formalism, it is not straightforward to impose the smallest possible length for plectonemes l_c, which leads to a systematic overestimation of the mean number of plectonemes due to the counting of unphysically small plectonemic regions. However, it is possible to correct this overestimation by calculating the fraction of plectonemes below the length cutoff from the theoretical plectoneme length distribution. After applying the correction, the results of the MP and TM models are found to be in excellent agreement. Details are provided in Appendix C. The advantage of the TM approach is that it has a simpler analytical structure than the MP model. As a consequence, this model permits the analytical description of quantities that cannot be derived directly from the MP model. An example of this is the characteristic plectoneme length ξ (see discussion in Appendix C).

III. MONTE CARLO SIMULATIONS

We performed Monte Carlo (MC) simulations based on the elastic Hamiltonian of the twistable wormlike chain (TWLC) discretized to 10 bp (or 3.4 nm) per monomer. This model features only two free elastic parameters: the bending modulus A and the twist modulus C, which—following the general choice in this work—were set to 40 and 100 nm, respectively. Electrostatics and steric hindrance are modeled via hard sphere potentials of radius 2 nm associated with each monomer. This radius was chosen to mimic the behavior of DNA under physiological ionic conditions [47], i.e., roughly 150 mM monovalent salt. In previous work, this hard-sphere radius, in conjunction with the mentioned elastic constants, was found to yield the best agreement with experimental single-molecule measurements [18]. Configurations are generated via a series of cluster moves as described in [18]. Simulations are conducted in the fixed linking number ensemble. This is facilitated by detecting and subsequently rejecting topology-violating moves and by including repulsion planes (via hard-wall potentials) normal to the force director field, which move in tandem with the chain termini. Further details about the model are provided in Refs. [32] and [18].

All simulations were conducted for molecules of length 7920 bp, which translates into 792 beads at the aforementioned resolution and a contour length of $L = 2692.8$ nm. Six different forces were considered, ranging from 0.4 to 1 pN. For each force, we examined a range of supercoiling densities, from zero to values well beyond σ_p, the supercoiling density at which the entire chain is expected to be in the plectonemic phase. Configurations from two such simulations are depicted in Figs. 4(a) and 4(b).

Accurate sampling of quantities such as the mean number of plectonemes and the plectoneme length distribution requires generating uncorrelated configurations. At high supercoiling densities, where most of the molecular length is contained within plectonemic regions, rearranging plectonemes along the chain requires substantial confluence of individual Monte Carlo moves. Consequently, sampling—especially at large forces, where plectonemic coiling is tight—becomes very inefficient. Simulations effectively remain stuck in their given configurations for a large number of MC moves. The decrease in sampling efficiency due to enhanced coiling density induced by the force is illustrated in the kymographs of Figs. 4(c) and 4(d), which display the location of plectonemes as shaded regions. For $f = 0.5$ pN [Fig. 4(c)] the MC algorithm refreshes the distribution of plectonemic regions along the chain quite frequently, while

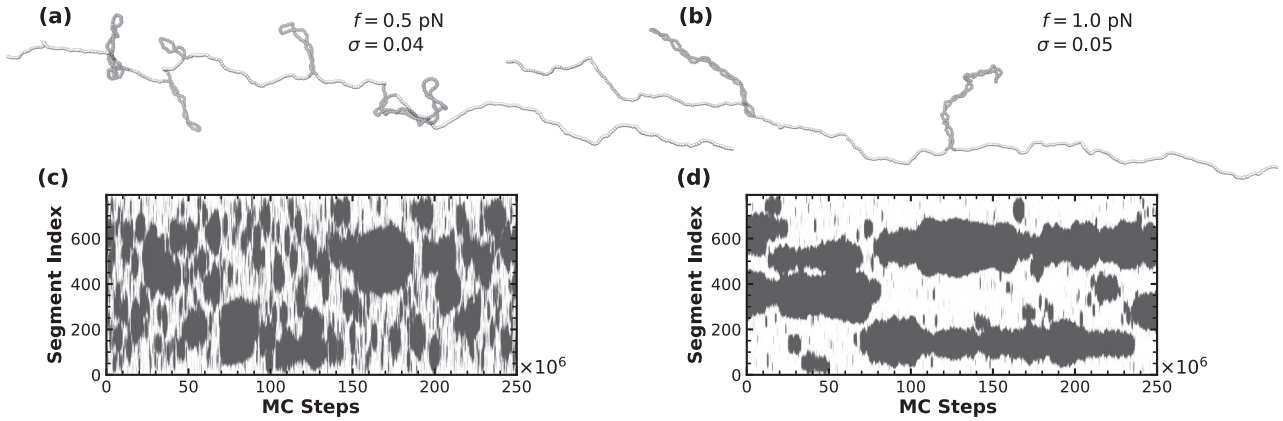

FIG. 4. Snapshots of configurations generated with MC simulations for molecules of 7920 bp (length $L = 2692.8$ nm) for (a) $f = 0.5$ pN, $\sigma = 0.04$ and (b) $f = 1.0$ pN, $\sigma = 0.05$. (c), (d) Kymographs showing the position of plectonemic domains (depicted as dark regions) for the full simulations from which the snapshots shown in panels (a) and (b), respectively, were taken. At $f = 0.5$ pN the algorithm facilitates frequent changes in the location and number of plectonemes, while large-scale configurational changes are difficult to attain at $f = 1.0$ pN.

the $f = 1$ pN [Fig. 4(d)] simulation exhibits only a handful of large-scale rearrangements.

To boost sampling efficiency, we employed an enhanced sampling method we term topological exchange sampling, which is similar to the approach used by Krajina and Spakowitz [48] to study the conformational statistics of supercoiled circular DNA. Simulations of all considered linking numbers corresponding to the same force are run concurrently. At regular MC step intervals, attempts are made to exchange configurations between neighboring linking number states. The linking number in the two corresponding configurations is adjusted uniformly by modifying the twist to fit the respective ensemble. Exchanges are accepted based on the usual Metropolis criterion. This type of configuration exchange allows highly congested configurations to migrate into low supercoiling density states, where configurational refreshing is efficient. Even with enhanced sampling, simulations of forces beyond 1 pN yielded poor statistics, which prompted us to limit the range of considered forces to this value.

A. Evaluation of Monte Carlo simulations

Plectonemic regions are identified based on their contribution to the total writhe of the configuration. Writhe is a quantity that measures the amount of coiling of a closed curve around itself. Large writhe density is therefore a differentiating property of plectonemic supercoils, setting them apart from the comparably low writhe density stretched phase. Mathematically, writhe is expressed as a double integral along a closed curve [12,49]. In the context of discrete chains, this can be reduced to a double sum [32,50]

$$\mathrm{Wr} = \sum_{i=1}^{N} \sum_{j=1}^{N} \omega_{ij}, \tag{28}$$

over the pairwise contributions ω_{ij}, representing double line integrals over pairs of straight segments (see Ref. [50] for details). We refer to previous work for a more detailed description of the plectoneme detection algorithm. As a final condition, we classify only those regions as plectonemes that contribute at least one unit of writhe.

Torque can be directly measured in simulations by constraining the rotational state of the last bead within a harmonic potential, similar to the torsional traps used to measure torque in magnetic torque tweezer experiments [37]. This method allows for precise control and measurement of torque. Alternatively, the average torque can be calculated from the twist strain using the formula:

$$\tau = \frac{2\pi k_{\mathrm{B}} TC}{L} \langle \Delta \mathrm{Tw} \rangle, \tag{29}$$

where ΔTw is the accumulative excess twist along the molecule. Experimentally, one is limited to the readout and manipulation of the magnetic bead, which does not provide access to the precise twist state of the molecule. In contrast, our simulations yield detailed information about the twist state and other properties, allowing us to deduce these by direct observation.

B. Number of plectonemes and torque

Data sampled with the MC simulations for the extension, mean number of plectonemes, and torque for the range of forces and supercoiling densities considered are displayed in Figs. 5(a)–5(c), respectively. The extension exhibits the well-documented quadratic decrease for small supercoiling densities—as described by the theory of chiral entropic elasticity [38]—followed by a nearly linear decrease in the post-buckling regime related to the conversion of stretched phase to plectonemes. Plectonemes are most numerous at low forces, see Fig. 5(b). For any given force, the number of plectonemes varies nonmonotonously with increasing supercoiling density. As expected, no plectonemes are observed for small σ (below the buckling point σ_s). Past the buckling point, this number steadily increases until a maximum is reached at a point roughly halfway through the postbuckling regime. This point corresponds to an extension reduction of about 50% relative to the relaxed state of the corresponding force ($\sigma = 0$). Beyond this maximum, $\langle n \rangle$ decreases steadily until

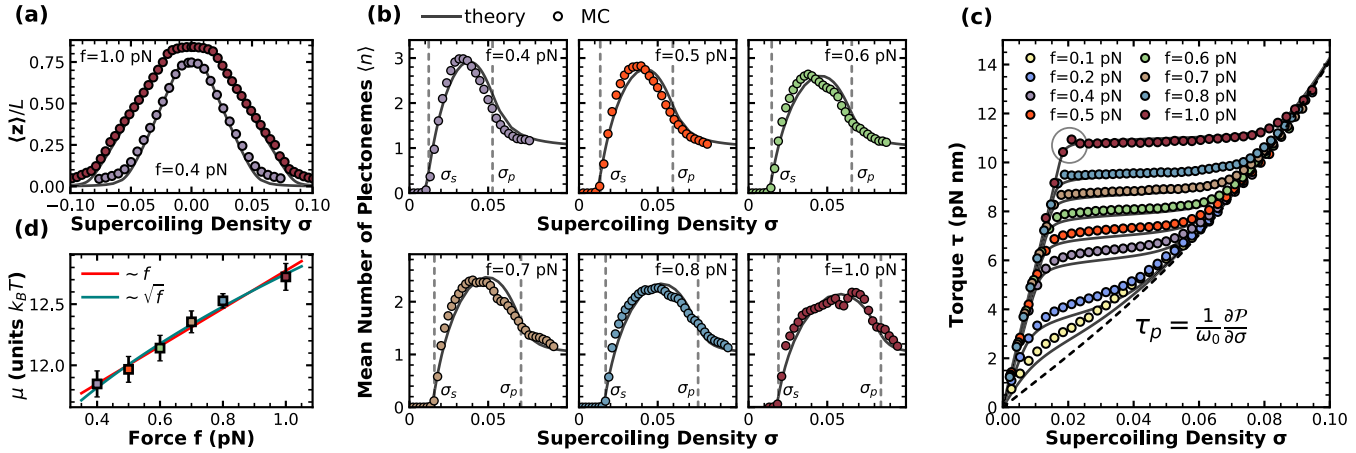

FIG. 5. (a)–(c) Summary of comparison of MC simulation data (circles) with the MP model of Sec. II (solid lines) for various quantities. Six different forces were simulated. The symbol colors in panels (a) and (b) follow the legend given in panel (c). (a) Average relative extension $\langle z\rangle/L$ vs σ. (b) Average number of plectonemes $\langle n\rangle$ vs σ. (c) Average torque $\langle\tau\rangle$ vs σ. (b) The plectoneme nucleation free energy μ is a free parameter in the MP model which can be obtained from fitting Eq. (24) to data of the average number of plectonemes. A plot of μ vs force is shown in panel (d).

eventually converging to $\langle n\rangle \to 1$ in the pure plectonemic phase. As outlined before, the best sampling is achieved for small forces and low supercoiling densities, while sampling becomes unreliable past the point of maximum number of plectonemes for $f = 1$ pN.

The torque varies linearly with σ in the prebuckling regime, see Fig. 5(c). Postbuckling, the torque response remains nearly flat at higher forces but shows a pronounced force dependence at lower forces. To highlight this force dependence, we included simulation data for forces as low as 0.1 pN. MT studies have reported an abrupt buckling transition, where the average extension sharply drops at the buckling point, and a torque "overshoot" [22,51], both of which have been predicted by both theory and simulations [44,52].

In our MC data, we observed a tiny signature of such torque overshoot at the highest force analyzed $f = 1.0$ pN, see encirclement in Fig. 5(c). The torque overshoot is related to the energy barrier crossing of plectoneme nucleation and is therefore a finite-size effect. Accordingly, it is most visible for short molecules (<2 kbp) and strong forces [44]. Lastly, we note that for all considered forces the torque appears to converge to a single curve once approaching the fully plectonemic state.

To compare the MP model to the MC simulations we invoke higher-order corrections to the free-energy densities of stretched and plectonemic phase [Eqs. (1) and (2)]. These corrections introduce two additional parameters that have been determined by independent free-energy calculations in previous work, see Appendix A and Ref. [32] for a deeper discussion.

The only remaining free parameters in the model are the smallest possible plectoneme size l_c and the plectoneme nucleation free energy μ, both of which can be determined from MC data. The value of l_c can be estimated from plectoneme length distributions obtained from MC simulations which will be discussed in detail in Sec. III C. Once l_c is fixed as a function of force, μ can be determined by fitting the model to the MC data.

In principle, any observable can be used for the fit, however, we find the number of plectonemes to be most sensitive to μ, therefore yielding the lowest uncertainty for the fitted parameter. The extension is found to be almost entirely insensitive to μ, while torque is only sensitive to μ for small forces, where the high-force expansion free energies [Eqs. (3) and (4)] become unreliable. There is, however, a caveat in employing $\langle n\rangle$ as a basis for fitting μ in that the MC results for $\langle n\rangle$ depend on the cutoff writhe used to classify plectonemes. This introduces an additional layer of uncertainty on μ. Regardless, $\langle n\rangle$ yields the most direct access to μ. As described above, we consistently used a cutoff value of one unit of writhe to classify plectonemes. Furthermore, numerical values of μ always defer to a particular choice of the discretization length Δl. Changing the discretization length from Δl to $\Delta l'$ in turn changes μ to μ' following

$$\mu' = \mu + 2k_{\mathrm{B}}T \log\left(\frac{\Delta l}{\Delta l'}\right). \tag{30}$$

In the above, the second term takes into account the gain and loss of entropy when changing the mesh size of the system. The resulting values of μ for individual stretching forces with $\Delta l = 1$ nm are displayed in Fig. 5(d). Previous work suggests μ to scale as $\sqrt{f}$ [43,44]. However, the relatively small range of forces considered does not permit us to discern this behavior from linear scaling. We, therefore, included fits for both types of scaling. We note that the values we find for μ cannot be directly compared with the tail-segment and end-loop energies calculated by Marko and Neukirch [44] because of the interpretational differences of the two approaches. We touch on these differences in more detail in Appendix B.

Observables calculated with the MP model using values of μ fitted from the average number of plectonemes are found to incorporate all the aspects observed in the MC data, short of the small torque overshoot for the 1 pN data [marked by a small gray circle in Fig. 5(c)]. As shown in the torque vs σ graph [Fig. 5(c)], the theory captures the deviations from a first-order transition that manifests in the nonconstant torque

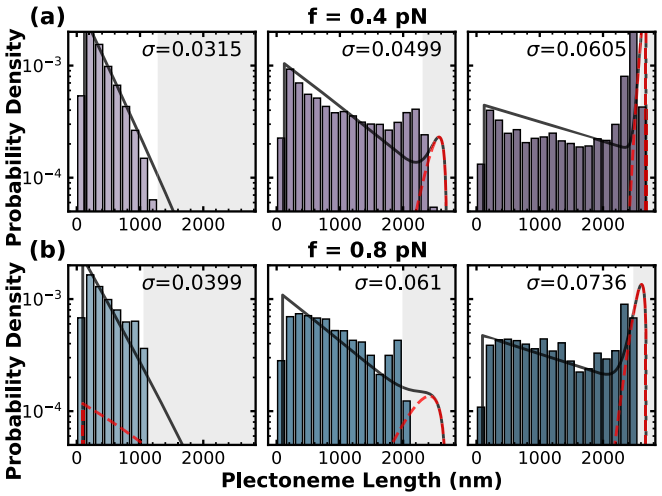

FIG. 6. (a), (b) Comparison of plectoneme length distributions from MC simulations (bars) and MP model as given by Eq. (27) (solid lines) for three different σ and (a) $f = 0.4$ pN, (b) $f = 0.8$ pN. The dashed red line shows the plectoneme length distribution of the subensemble with just one plectoneme. For small σ, plectonemes are short and the length distributions are rapidly decaying. For large σ, plectonemes are long and the distributions are peaked at lengths close to the total length of the DNA molecule. MC data hardly extend to lengths beyond L_p (gray area), given in Eq. (31). Distributions calculated with the MP model extend to the entire length of the molecule. This difference is due to the different ensembles used in the two calculations, see discussion in the text.

in the coexistence region, corresponding to τ^* of Eq. (11) in the quadratic model. For all forces, the torque curves are found to eventually converge to the torque curve of the plectonemic phase. This quantity can be obtained via differentiation of the plectoneme free energy and is shown as a dashed line in Fig. 5(c). The curvature of τ_p is a direct indication of the breakdown of the quadratic approximation for $\mathcal{P}(\psi)$ and justifies the requirement of a quartic free energy extension, see Eq. (A1).

C. Plectoneme length distribution

Plectoneme length distributions obtained from MC simulations (bars) and the MP model (solid lines) are shown in Figs. 6(a) and 6(b). The data correspond to three separate supercoiling densities σ for two different forces: (a) $f = 0.4$ pN and (b) $f = 0.8$ pN. The theoretical curves of the MP model are plotted using the corresponding values of μ [see Fig. 5(d)], whereas l_c is obtained from the sharp drop of the plectoneme length distributions obtained for small plectoneme lengths (see Appendix D for details). While the theory predicts a nonzero probability of finding plectonemes of the longest possible length, i.e., the length of the entire molecule, the simulations exhibit a sharp probability dropoff around a particular and supercoiling density-dependent length. This discrepancy stems from the difference in the considered ensemble. The simulations are conducted in the fixed linking number ensemble, where, for a given σ , the length fraction stored in the plectonemic state is expected to be [32,39]

$$L_p = (1 - \langle \nu \rangle)L = \frac{\sigma - \sigma_s}{\sigma_p - \sigma_s} L. \tag{31}$$

Unless σ is close to σ_p, the probability of L_p to fluctuate to L is exceedingly unlikely (for details see, e.g., Ref. [32]). The theory, on the other hand, is derived in the fixed torque ensemble, which permits linking number fluctuations. Since torque differences are generally small [except for the smallest of forces; see Fig. 4(c)], linking number fluctuations can be large, allowing plectoneme length fluctuations over the entire possible range. The gray shaded region in Figs. 6(a) and 6(b) indicates plectoneme lengths above L_p, confirming Eq. (31) to provide an upper bound to plectoneme length fluctuations observed in MC simulations.

For plectoneme lengths below L_p we find reasonable agreement between the MC data and the MP model. For relatively short plectonemes, the theory predicts an exponential plectoneme length distribution. The corresponding decay length ξ constitutes the characteristic plectoneme length. While the exponential decay cannot be directly derived from the MP model due to its complex analytical structure, it can be obtained analytically using the TM approach (see Appendix C). The predicted characteristic plectoneme length from the TM theory is in line with the results obtained from MC simulations (as discussed extensively in Appendix C).

For sufficiently large σ both theory and simulation display a peak in the probability density close to the largest observed length. This peak can be explained by considering plectoneme length distributions within subensembles of a fixed plectoneme number. The dashed line shows the corresponding distribution for the subensemble containing only a single plectoneme, which illustrates that the peaks are a result of these subensemble states.

IV. COMPARISON WITH EXPERIMENTS

The MC simulations used in this work were parametrized to match linking number-dependent surface-bead distances and variances measured with single-molecule magnetic tweezers for 7.9 kb DNA tethers, see Ref. [18] for details. An interesting prediction of the theory and the MC simulations is the nonflat torque response observer for low forces in particular (also predicted by Emanuel *et al.* [43]). We compare these results with optical tweezer measurements of DNA tethers reported by Gao *et al.* [45]. Figure 7 shows the relation of torque vs supercoiling density for forces ranging from 0.25 to 5 pN. The model developed in this paper (black line) is coplotted with the experimental data (colored lines). To produce the solid lines of Fig. 7 the MP model was used, choosing $A = 43$ nm and $C = 109$ nm, as reported in Gao *et al.* [45]. In addition, we used an alternate parametrization of the plectoneme free energy by setting the coefficient of the quadratic term $P_2 = 20$ nm (see Appendix A). This is higher than the value $P_2 = 14.4$ nm used throughout the rest of the paper. Notably, the value of $P_2 = 20$ nm is very close to the value of the effective torsional stiffness for the lowest measured force in Ref. [45].

While it is difficult to observe a signature of multiplectonemes from the higher forces, the $f = 0.25$ pN data are

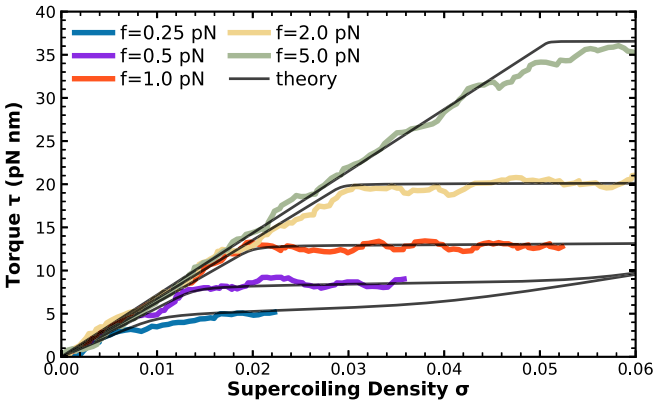

FIG. 7. Comparison between experimental measurements (symbols) of torque in function supercoiling density and the results from the MP model (solid lines), as obtained by inverting Eq. (23). For the theoretical curves, we used $A = 43$ nm and $C = 109$ nm as reported in Ref. [45]. The plectoneme free energy was parameterized using $P_2 = 20$ nm and $P_4 = 520$ nm. Experimental data are from Ref. [45], courtesy of M. Wang.

found to closely align with the MP model. Unfortunately, due to technical issues arising when the magnetic bead comes into proximity with the flow cell surface, the experimental data are limited to comparably small values of σ. It would be interesting to experimentally verify the torque response in a wider range of supercoiling density to corroborate the convergence into a single torque curve as predicted by the theory. Such a measurement would give direct access to the free-energy landscape of the plectoneme phase.

Lastly, we turn to a set of experimental data that gives direct access to plectoneme statistics. Van Loenhout *et al.* [25] developed an MT setup that allows for the sideway pulling of fluorescently labeled DNA molecules and the subsequent visualization of the DNA contour via epi-fluorescence. Plectonemes appear as bright spots as they correspond to regions of high DNA density. Using this setup, it is possible to locate plectoneme positions and follow their dynamics in real time. The quoted study used 21 kb DNA molecules. We first verify the validity of our theory vis-à-vis the experimental data by comparing measured and theoretical extension as a function of applied force and supercoiling density, see Fig. 8(a). The theoretical curves were constructed with the same parameters as used to compare to MC data. The observed agreement attests to the quality of the model parametrization.

Average plectoneme numbers $\langle n \rangle$ vs applied force are shown in Fig. 8(b). Experimentally considered supercoiling densities were specifically selected such that 25% of the DNA length is contained in the plectonemic phase [see circles in Fig. 8(a)]. We used the MP model to compare the average number of plectonemes $\langle n \rangle$ to the experimental data of Ref. [25]. Values of μ and l_c are chosen by extrapolating the $\sqrt{f}$ fit from Figs. 5(d) and 13(b), respectively. To ensure comparability to experiments, the MP model was evaluated at torques for which L_p amounted to 25% of the DNA molecule's contour length. Figure 8(b) indicates the theory (solid line) to predict a considerably larger number of plectonemes for the experimentally considered molecule length and force and supercoiling density conditions than experimentally observed.

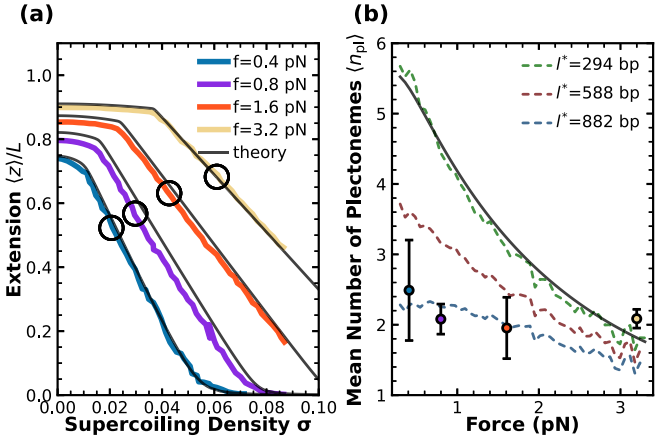

FIG. 8. (a) Comparison between experimental force-extension curves (symbols) taken from Ref. [25] and results obtained from the MP (solid lines) for a 21 kb DNA. The circles indicate the conditions under which the fluorescence measurements were performed. (b) Mean number of plectonemes as a function of force obtained from fluorescence microscopy measurements [25] and according to the MP model from Eq. (24). Dashed lines are obtained from Monte Carlo sampling the MP model (MC-MP) in conjunction with a minimal plectoneme detection length l^* (thus plectonemes of lengths $l > l_c$ are generated, but only those with length $l > l^*$ are counted in the calculation of $\langle n \rangle$). Results indicate that the experimental resolution of Ref. [25] is limited to plectonemes of about 1 kb in length. For the MP model and the MC-MP we used $A = 40$ nm, $C = 100$ nm, $P_2 = 14.4$ nm, and $P_4 = 520$ nm as for the MC simulations in Fig. 5. The small differences between these parameters and those used to fit the data of Gao *et al.* [45] (Fig. 7) might be related to the difference in buffer conditions of the two experimental setups.

This result is consistent with previous Monte Carlo simulations by Lepage *et al.* [27]. Moreover, the MP model predicts the mean number of plectonemes $\langle n \rangle$ to decay rapidly with the applied tension f, while experimental observation suggests much lower force dependence.

This discrepancy might be attributed to the limited experimental resolution, which does not allow for the observation of short plectonemes. To further investigate the typical plectoneme detection limit in the experiment, we sampled MP model configurations using a Monte Carlo algorithm (referred to as MC-MP). This algorithm starts from a DNA chain that is fully in the stretched phase. Its configuration is updated by either randomly selecting a single site and changing its state from the S(P)-phase to P(S)-phase or by selecting a range of sites and changing their states collectively. Moves that generate plectoneme domains smaller than l_c are immediately rejected. Otherwise, changes made are accepted/rejected according to the Metropolis rule. The dashed colored lines in Fig. 8(b) are MC-MP simulation data in which a cutoff length l^* is used to detect plectonemes, meaning that only plectonemes of length longer than l^* are considered in the determination of $\langle n \rangle$. As shown in Fig. 8(b), the MC-MP data is in reasonable agreement with experiment when a minimal plectoneme detection length of $l^* = 0.9$ kb is used. Under these conditions, the theory predicts the average number of plectonemes to be weakly dependent on force, as is apparent from the experimental data. This potentially suggests the

fluorescence measurements to be sensitive only to plectonemes of size larger than approximately ≈1 kb, while shorter plectonemes may evade detection. This effect would be most prominent for small forces, where plectonemes are preferentially short and numerous.

V. CONCLUSION

In this paper, we presented the results of MC simulations of stretched and torsionally constrained DNA, modeled as a bistable wormlike chain. DNA molecules were represented as a series of coarse-grained beads (each corresponding to 10 bp) characterized by bending and torsional stiffnesses, chosen to reproduce experimental data of bending and torsional persistence lengths. We analyzed the statistical properties of plectonemes, which form along the molecule once it is over- or underwound. Using an algorithm developed in prior work [32], we detected the number of plectonemes and their lengths for configuration snapshots from an MC-generated equilibrium ensemble at a fixed linking number and stretching force. In parallel, we developed a statistical mechanical model of stretched supercoiled DNA which we referred to as MP model. This model is a simple extension of the two-phase model of Marko [39]. An excess free-energy term is introduced as the penalty for the interface between a stretched DNA and a plectonemic domain. All parameters of the MP model, except the phase boundary free energy and plectoneme length threshold, were determined in prior studies that focused on other properties of supercoiled DNA [18,32]. The two-phase model was proven to capture several features of stretched and torsionally constrained DNA [39], including extension fluctuations [18,32]. Here we showed the model to quantitatively reproduce multiple features observed in simulations, such as the average number of plectonemes and their length distribution. The agreement with simulations is remarkable because the model contains only two adjustable parameters, which makes it more accessible than more sophisticated approaches proposed in the prior literature [43,44]. We have also discussed a simpler transfer matrix-based approach, which is in good agreement with the full model, see Appendix C.

The main difference between our theoretical approach and previous such attempts is the use of a phenomenological plectoneme free energy in the form of a quartic polynomial. Previous approaches used more detailed geometric descriptions accounting for elastic, entropic, and electrostatic contributions [43,44]. A discussion of these terms is given in Appendix B, which also shows a comparison with the phenomenological free energy employed in this paper. The microscopic and phenomenological free energies are in good quantitative agreement, but stronger deviations are observed at small supercoiling densities, a regime in which plectonemes are loose and highly fluctuating in shape. Constructing a good quantitative microscopic model in this regime remains challenging.

ACKNOWLEDGMENTS

Discussions with Pauline Kolbeck, Jan Lipfert, and Willem Vanderlinden are gratefully acknowledged. M.S. acknowledges financial support from Fonds Wetenschappelijk Onderzoek-Vlaanderen (FWO) Grant No. 11O2325N. E.S. acknowledges financial support from Fonds Wetenschappelijk Onderzoek-Vlaanderen (FWO) Grant No. 1SB4219N. E.S. and H.S. were supported by the Deutsche Forschungsgemeinschaft (DFG, German Research Foundation) under Germany's Excellence Strategy–EXC-2068–390729961.

APPENDIX A: HIGHER-ORDER EXTENSIONS

For the analysis of simulation data, we extended two features of the free energies (1) and (2). We added a quartic term in the supercoiling density ψ of the plectonemic free energy, which was extended as follows:

$$\mathcal{P}(\psi) = \left(\frac{P_2}{2}\psi^2 + \frac{P_4}{4}\psi^4\right)\omega_0^2 k_B T. \tag{A1}$$

The coefficients P_2 and P_4 were fitted to MC simulation data in Ref. [32], using umbrella sampling and suitable boundary conditions to induce a pure plectonemic phase. As the supercoiling density ψ is dimensionless P_4 and P_2 in (A1) have units of length. Fitted free energies give $P_2 = 14.4 \pm 0.3$ nm and $P_4 = 520 \pm 30$ nm [32]. It was not necessary to extend the stretched phase free energy $\mathcal{S}(\phi)$ given in (1), beyond the quadratic term in ϕ. This is because stretched segments attain a maximum value $\phi \approx \sigma_s \ll \sigma_p$. The need for a quartic term in (A1) arises from the fact that plectonemes are characterized by a large supercoiling density. However, we extended Eq. (3) to the next order in the force f to better account for the low-force regime. We used the following expansion [32]:

$$g(f) = f\left(1 - \sqrt{\frac{k_B T}{Af}} + g_2\frac{k_B T}{Af}\right). \tag{A2}$$

Reference [32] reports $g_2 = 0.3$, obtained from the numerically exact solution of a stretched wormlike chain [53] where we took $A = 40$ nm and $k_{B\pm}T = 4.1$ pN nm, corresponding to room temperature. Note that the term proportional to g_2 contributes to the stretched phase free energy as an overall force-independent constant. This is important for the double tangent construction because it gives a constant relative shift to the stretched- and plectoneme-phase free energies.

APPENDIX B: COMPARISON WITH OTHER THEORIES

In this paper, we employed a phenomenological form of the plectonemic free energy, which contains quadratic and quartic terms in the supercoiling density, see (A1). In other studies [43,44], the plectonemic free energy is derived from a microscopic description of DNA supercoils. These models assume that DNA supercoils can be adequately represented as geometrically ideal superhelices characterized by a superhelical radius r and an opening angle α. We compare here the phenomenological free energy (A1) with the model by Marko and Neukirch [44]. As (A1) describes the bulk free energy per unit length of a very long plectoneme, we compare it to that reported in Ref. [44], neglecting finite-size effects such as end-loop contributions. In this limit, the plectoneme free

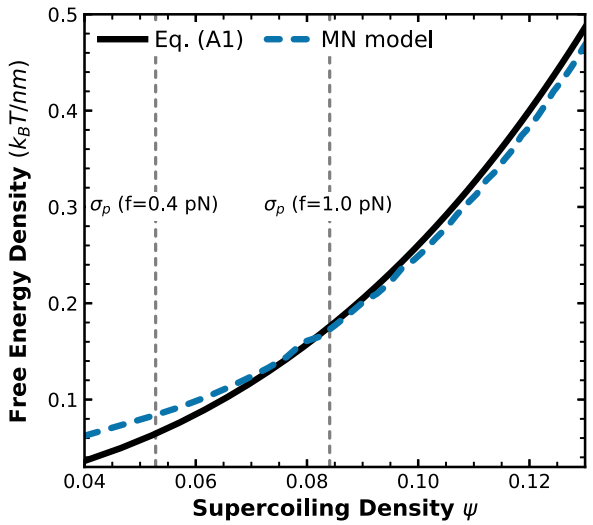

FIG. 9. Comparison between Eq. (A1), the phenomenological plectonemic free energy (solid, black), and Eq. (B2), the free energy obtained from the microscopic model of Marko and Neukirch (MN) (dashed, blue). The parameters of the phenomenological free energy are $P_2 = 14.4$ nm and $P_4 = 520$ nm, as used throughout this work. The gray dotted lines indicate σ_p for a stretching force of 0.4 and 1 pN, indicating that the discrepancies of the microscopic model become more important for small stretching forces. For the MN theory, we used the parameters $A = 40$ nm, $l_B = 0.7$ nm, $\nu = 8.8558\ \text{nm}^{-1}$ and $k_D^{-1} = 0.79$ nm, mimicking a salt concentration of 150 mM monovalent salt and a temperature of 296.5 K, as reported in Ref. [44].

energy per unit length of the Marko-Neukirch model is [44]

$$\begin{aligned}\beta\mathcal{P}_{\text{MN}}(\psi, r, \alpha) &= 2\pi^2 C\Big[\frac{\omega_0}{2\pi}\psi - w_p(r,\alpha)\Big]^2 \\ &\quad + A\frac{\sin^4(\alpha)}{2r^2} + l_B\nu^2 K_0(2k_D r) + \frac{r^{-2/3}}{2A^{1/3}}. \end{aligned} \tag{B1}$$

The first term describes the energetic cost associated with twisting of the DNA molecule, with $\omega_0\psi/2\pi$ the excess linking number per unit length and w_p the writhe per unit length of a regular superhelix (as in the rest of the paper C denotes the DNA torsional stiffness). The second term, proportional to the bending stiffness A, describes the energetic bending cost. The third term is the electrostatic repulsion with K_0 the modified Bessel function of zeroth order, $l_B = 0.7$ nm the Bjerrum length, $\nu = 8.8558\ \text{nm}^{-1}$ the effective charge and $k_D^{-1} = 0.79$ nm the Debye length. Finally, the last term is the entropic confinement contribution to the free energy [3,54]. In order to obtain the plectonemic free energy as a function of supercoiling density, Eq. (B1) is minimized with respect to r and α

$$\overline{\mathcal{P}}(\psi) = \min_{\alpha,r} \mathcal{P}_{\text{MN}}(\psi, r, \alpha). \tag{B2}$$

The results of this minimization are shown in Fig. 9 (dashed, blue) together with (A1) the phenomenological free energy used throughout this work (solid, black). There is good agreement between the two free energies at high supercoil densities, while some deviations are observed at low supercoil densities $\psi < 0.07$. The typical plectonemic supercoiling density can be estimated from the values of σ_p obtained from the two-phase model double tangent construction or from the coexistence condition in the torque ensemble $\widetilde{\mathcal{S}}(\tau^*) = \widetilde{\mathcal{P}}(\tau^*)$. The values for σ_p for two forces are shown in Fig. 9 as vertical dashed lines. The discrepancies between the variational free energy (B2) and the phenomenological one (A1) are probably due to the former underestimating the plectoneme's entropy. At low supercoiling densities, a plectoneme is loose, and its description as a regular superhelix with well-defined values for radius r and angle α may break down. Such description seems to be more accurate at high supercoiling densities when plectonemes are tight and fluctuations less relevant.

Marko and Neukirch [44] further provided an empirical formula for the combined energetic cost of the plectoneme end loop and the tail segments [see last term in Eq. (5) of their work]. Unfortunately, this energetic cost may not be directly compared to the interface term μ from the present work as the former contains contributions that are already implicitly contained in the effective plectoneme free energy $\mathcal{P}(\sigma_p)$. It is not obvious how these contributions can be disentangled, and any such attempt, short of the careful analysis of the geometry and local energetics of the MC generated configurations, would be subject to crude assumptions that render any drawn conclusions overly circumstantial. Such analysis goes far beyond the scope of the current work and could be the subject of a dedicated study.

APPENDIX C: TRANSFER-MATRIX APPROACH

An alternative approach to the multiplectonemic-phase free energy is based on the following 2×2 transfer matrix (TM):

$$T = \begin{pmatrix} s & wp \\ ws & p \end{pmatrix}, \tag{C1}$$

where s and p are the weights of the two phases

$$\begin{aligned} s &= \exp(-\beta\Delta l\widetilde{\mathcal{S}}), \\ p &= \exp(-\beta\Delta l\widetilde{\mathcal{P}}), \end{aligned} \tag{C2}$$

corresponding to a discretization length Δl. The term $w < 1$ is the additional weight associated with the interface between stretched and plectonemic segments. This is linked to the interfacial free energy μ of (13) through the relation

$$w = e^{-\beta\mu/2}, \tag{C3}$$

assuming the same choice of Δl as in the multiplectoneme model. For different choices of Δl, μ rescales according to Eq. (30), see discussion below.

This TM approach is identical to the Zimm-Bragg model used to describe the helix-coil transition in polypeptides [55] and is also often used to describe two-state transitions of single molecules; see, e.g., Ref. [56] for a recent example. The TM matrix multiplication generates the Boltzmann weights of all possible configurational permutations of stretched and plectonemic segments. For example, a configuration containing two plectonemes of size $m\Delta l$ and $q\Delta l$ (separated by a stretched phase of length $r\Delta l$) has weight

$$s^k w p^m w s^r w p^q w s^t, \tag{C4}$$

with two stretched segments of length $k\Delta l$ and $t\Delta l$ at the ends of the molecule. The integers k, m, r, q and t are such

that $k+m+r+q+t=N$ with $N\Delta l$ the total length of the DNA. In the calculation, we impose two stretched segments at the two ends of the molecule. This choice of boundary condition reflects the MT setup in which the tethering of the DNA to the bead and the surface imposes certain constraints inhibiting the nucleation of plectonemes at the DNA termini. The corresponding stretched-stretched partition function for a molecule of length $N\Delta l$ is given by

$$Z_{ss}(N) = s(1 \quad 0)T^{N-1}\begin{pmatrix}1\\0\end{pmatrix} = \frac{s-\lambda_-}{\lambda_+-\lambda_-}s\lambda_+^{N-1} + \frac{\lambda_+-s}{\lambda_+-\lambda_-}s\lambda_-^{N-1}, \tag{C5}$$

where $\lambda_\pm$ are the eigenvalues of T,

$$\lambda_\pm = \tfrac{1}{2}\{s+p \pm \sqrt{(s-p)^2+4w^2sp}\}. \tag{C6}$$

To obtain (C5), we used the decomposition

$$\begin{pmatrix}1\\0\end{pmatrix} = \frac{1}{wp}\left[\frac{s-\lambda_-}{\lambda_+-\lambda_-}\mathbf{v}_+ + \frac{\lambda_+-s}{\lambda_+-\lambda_-}\mathbf{v}_-\right], \tag{C7}$$

where

$$\mathbf{v}_\pm = \begin{pmatrix}wp\\ \lambda_\pm - s\end{pmatrix}, \tag{C8}$$

are the eigenvectors of T corresponding to the eigenvalues $\lambda_\pm$. Using some elementary algebra from (C5), one gets for $N \leqslant 4$: $Z_{ss}(1)=s$, $Z_{ss}(2)=s^2$, $Z_{ss}(3)=s^3+s^2pw^2$ and $Z_{ss}(4)=s^4+2s^3pw^2+s^2p^2w^2$, showing that with the stretched-stretched boundary conditions, a plectoneme can appear only for lengths $N \geqslant 3$ and has maximal length $(N-2)\Delta l$. For very high supercoiling densities $\sigma \gg \sigma_p$ [or $p \gg s$ and $\lambda_+ \approx p + w^2sp/(p-s)$, $\lambda_- \approx s - w^2sp/(p-s)$, neglecting higher order terms in w^2] the partition function is dominated by a single term $Z_{ss} \approx s^2p^{N-2}w^2$.

In the TM formalism the free energy per unit length in the thermodynamic limit is given by

$$\widetilde{\mathcal{F}} = \lim_{N\to\infty}\frac{-k_BT\log Z_{ss}}{N\Delta l} = -\frac{k_BT}{\Delta l}\log\lambda_+. \tag{C9}$$

One can get the supercoiling density σ by means of a torque derivative, see Eq. (23). An expression for the average number of plectonemes can be obtained by differentiation with respect to w^2, i.e.,

$$\langle n\rangle = w^2\frac{\partial \log Z_{ss}}{\partial w^2}. \tag{C10}$$

This follows from the fact that each plectoneme comes with an interfacial weight w^2, therefore counting the plectonemes is equivalent to counting the powers of w^2 in every Boltzmann weight in Z_{ss}. For instance, the weight (C4) is proportional to w^4, corresponding indeed to two plectonemes. Note that the stretched-stretched boundary conditions impose that only terms with even powers of w enter in the partition function.

The probability of finding a plectoneme of length $m\Delta l$ embedded within a segment of stretched phase is given by

$$P_{\rm pl}(m) = \frac{1}{Z^*_{ss}(N)}\sum_{k=1}^{N-m-1} Z_{ss}(k)w^2p^mZ_{ss}(N-k-m), \tag{C11}$$

where $k\Delta l$ is the entry point of the plectoneme along the curvilinear length and $Z_{ss}(k)$ is given by (C5). We use the partition function

$$Z^*_{ss}(N) = \sum_{m=1}^{N-2}\sum_{k=1}^{N-m-1} Z_{ss}(k)w^2p^mZ_{ss}(N-k-m), \tag{C12}$$

so that the distribution is properly normalized; $\sum_{m=1}^{N-2}P_{pl}(m)=1$. If plectonemes are shorter than the whole molecule length, the distribution decays rapidly, and the sum is dominated by the terms $N-k \gg m$ and $k \gg m$. Approximating $Z_{ss}(k) \sim \lambda_+^k$, $Z_{ss}(N-k-m) \sim \lambda_+^{N-k-m}$ one finds the plectoneme lengths to be exponentially distributed

$$P_{\rm pl}(m) \sim \left(\frac{p}{\lambda_+}\right)^m = e^{-m\Delta l/\xi}, \tag{C13}$$

where the characteristic length ξ is given by

$$\xi = \frac{\Delta l}{\log(\lambda_+/p)}. \tag{C14}$$

At the buckling point $\tau=\tau^*$ one has $s=p$ and therefore $\lambda_+ = p(1+w)$. The decay length (C14) becomes

$$\xi = \frac{\Delta l}{\log(1+w)} \approx \frac{\Delta l}{w}, \tag{C15}$$

where we used $w \ll 1$, i.e., the interface between the straight and plectonemic phases has a high energy cost and thus very low probability. The previous equation shows how the interfacial weight w can be obtained from the decay of the plectonemes length distribution at the buckling point $\tau=\tau^*$.

To understand the discretization length dependence in Eq. (C3), we can use the TM multiplication as follows. Let us consider starting from a given discretization length a and indicate with s, p, and $w(a)$ the weights corresponding to this choice of length. The TM multiplication k times gives

$$T^k \approx \begin{pmatrix}s^k & w_1(ka)p^k\\ w_2(ka)s^k & p^k\end{pmatrix}, \tag{C16}$$

where we kept the lowest terms in $w(a)$, giving

$$w_1(ka) = w(a)\left(1+\frac{s}{p}+\cdots+\frac{s^{k-1}}{p^{k-1}}\right), \tag{C17}$$

$$w_2(ka) = w(a)\left(1+\frac{p}{s}+\cdots+\frac{p^{k-1}}{s^{k-1}}\right). \tag{C18}$$

Via block decimation, the production in (C16) defines a new model with discretization length ka. In this model, the interfacial weight for going from the stretched phase to the plectonemic phase, w_1, is different from the one going from the plectonemic to the stretched phase, w_2. Since all configurations satisfying the stretched phase boundary conditions require the interfacial weights w_1 and w_2 to appear in pairs, what matters is the average Boltzmann weight defined as

$$w(ka) \equiv \sqrt{w_1(ka)w_2(ka)}. \tag{C19}$$

Close to buckling, $\tau \approx \tau^*$, the free energies of the stretched and plectonemic phases are degenerate, hence $s \approx p$ and $w_1(ka) \approx w_2(ka) \approx kw(a)$ and thus

$$w(ka) \approx kw(a). \tag{C20}$$

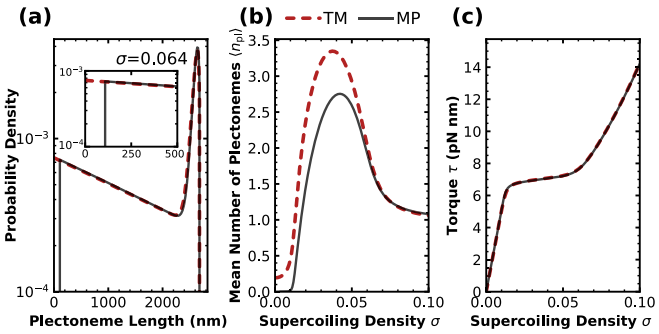

FIG. 10. Comparison of the multiplectoneme model (MP, solid lines) and the transfer matrix model (TM, dashed line). All curves were calculated for the same values of the stretching force $f = 0.5$ pN. (a) Plectoneme length distribution $P_{\rm pl}(l)$ vs. length l in lin-log scale. The inset zooms in on the short plectoneme length regime in which $P_{\rm pl}(l)$ of the TM model deviates from the MP model. The MP model does not take into account plectonemes shorter than some threshold length l_c, whereas the TM model allows all plectoneme lengths larger than the discretization length Δl. (b) Average number $\langle n\rangle$ of plectonemes vs σ. (c) Torque τ vs σ.

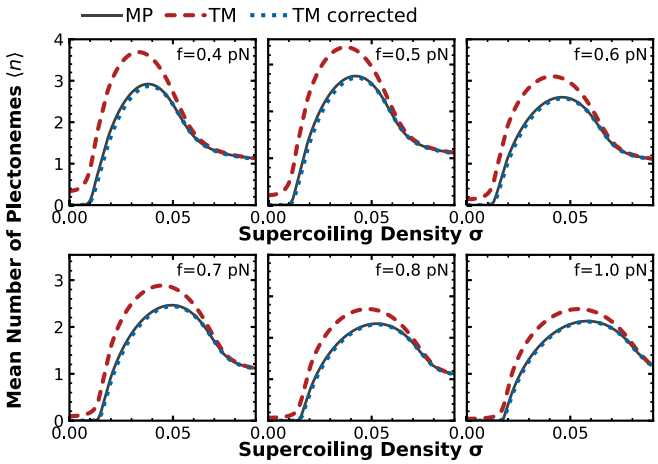

FIG. 11. Mean number of plectonemes according to the MP model (solid) and the TM model with (dotted) and without (dashed) the correction η [Eq. (C21)] for various forces.

This relation is equivalent to Eq. (30) and has a simple interpretation: The multiplicative factor k accounts for the number of different positions in which the interface between stretched and plectonemic phases can be placed in a discretized segment of length $\Delta l = ka$. This implies that the weights of individual segments must scale with the discretization length, $w(\Delta l) \propto \Delta l$. Note that this dependence cancels the Δl factor in the numerator in (C15).

Figures 10(a)–10(c) show a comparison of plectoneme length distribution $P_{\rm pl}(l)$, the average number of plectonemes $\langle n\rangle$ and torque vs supercoiling density as obtained from the multiplectoneme model (MP) and the TM formalism approach. As discussed in the text, the former method allows a direct incorporation of a minimal threshold length for a plectoneme l_c allowing for the discrimination of short unphysical plectonemic domains. However, in the TM formalism, plectonemes of all lengths above the discretization length Δl are generated. This can be seen in Fig. 10(a): the two models predict identical length distributions, except for deviations at small l where the TM approach (dashed line) predicts nonvanishing probability down to the smallest possible length scale (Δl). Conversely, the introduction of the cutoff length l_c excludes such small lengths in the probability distributions calculated with the MP model (solid line). The TM model predicts a larger average number of plectonemes as compared to the MP model [Fig. 10(b)] because the former counts very short plectonemes, which are not generated in the MP model. Both models are found to yield very similar estimates of supercoiling densities σ, see Fig. 10(c), as short plectonemes have negligible influence on global thermodynamic quantities. Moreover, we note the TM model and MP model yield identical results if the minimum plectoneme length l_c of the MP model is set to equal the discretization length Δl of the TM model, provided Δl is sufficiently small to adequately capture positional entropy. Unfortunately, this requirement is only satisfied for unphysically small values of l_c.

One can account for the overestimation of the mean number of plectonemes in the TM model by introducing a torque-dependent correction factor η which we define as

$$\eta(\tau) \equiv \int_{l_c}^{L} P_{\rm pl}^{(\rm TM)}(l,\tau)\mathrm{d}l. \tag{C21}$$

By integrating the TM model length distribution function from l_c to L, one excludes non-physical short plectonemes. We note that, as the plectoneme length distribution is normalized, one has $\eta(\tau) \leqslant 1$. The corrected average number of plectonemes is defined as

$$\langle n\rangle^* \equiv \eta\langle n\rangle. \tag{C22}$$

This is expected to be a good approximation as long as length correlations between distinct plectonemes can be neglected. Figure 11 shows a comparison of the predicted mean number of plectonemes from the MP and TM models, with and without the correction factor. The inclusion of η brings the predictions into excellent agreement.

While the MP model is more appropriate to describe the physics of the multiplectoneme phase, it has a more complex analytical structure as it requires the calculation first of the partition function of n plectonemes $Z(n)$ from (18) which is then summed over all n to get $Z_{\rm TOT}$, see Eq. (21). The TM on the other side is simpler to handle as the thermodynamic quantities are obtained from suitable derivatives of its eigenvalues $\lambda_\pm$. As the TM and the MP model predict the same decay of plectoneme length distribution, we employed the latter [Eq. (C14)] to compute the decay length ξ for various forces and supercoiling densities σ and compared them with those calculated with the Monte Carlo simulations. The results are plotted in Fig. 12 and show good overlap between theory and MC simulations.

APPENDIX D: MINIMAL PLECTONEME SIZE l_c

The MP model has two free parameters, the plectoneme nucleation free energy μ and the minimal length of a plectoneme l_c. The introduction of the latter is important to avoid

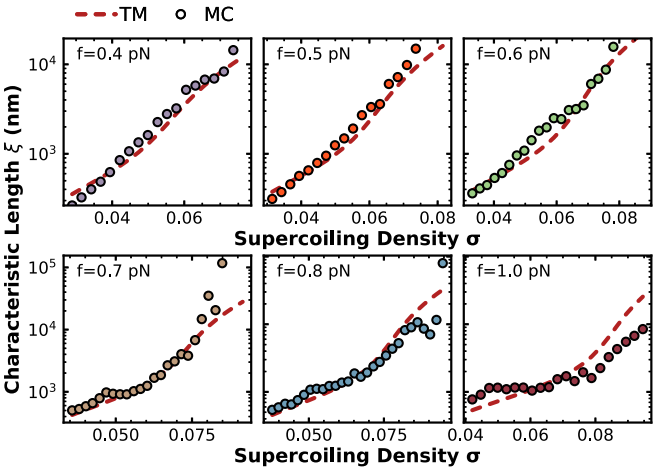

FIG. 12. Plots of force-dependent characteristic decay lengths ξ. Scatters indicate the values obtained by fitting the exponential decay of the length distributions obtained with the MC simulations, and the dashed lines show the theoretical predictions according to Eq. (C13).

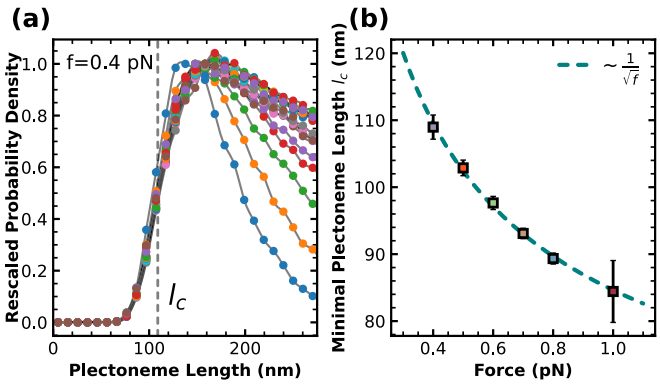

FIG. 13. (a) Plectoneme length distribution for a stretching force of 0.4 pN for supercoiling densities in the interval [0.021, 0.0815] as obtained from MC simulations (circles) along with interpolating cubic splines (dashed lines). The length distributions are rescaled to align at their local maxima. The minimal plectoneme length l_c is chosen as the mean-half maximum of the length distributions for a given force. (b) Force dependence of l_c. The error bars indicate the standard deviation of l_c determined for different supercoiling densities. The dashed line indicates the result of fitting Eq. (D1) to the deduced values of l_c.

consideration of very short plectonemic domains that would be unphysical as the classification of such a domain requires the formation of at least one loop. We determined values of l_c in a force-dependent manner based on the MC simulations. At short lengths [see Fig. 13(a)], the length distributions rise sharply at well-determined values, independent of supercoiling density, but depending on the stretching force. We extract the value of l_c by fitting a cubic spline through the initial rise of the probability density and extracting the value of the length at which $P_{\rm pl}(l)$ reaches half of its first local maximum. Following this procedure, the force dependence of l_c was obtained [see Fig. 13(b)]. To allow for the inter- and extrapolation of l_c we fitted the available values of l_c as a function of f with an empirical equation of the form:

$$l_c(f) = x_0 + x_1\sqrt{\frac{k_{\rm B}T}{Af}}, \tag{D1}$$

where the numerical constants x_0 and x_1 were found to be 41 and 134 nm, respectively. We note that the scaling of l_c with $1/\sqrt{f}$ is in agreement with the scaling of the plectoneme loop size [44].

[1] D. A. Koster, A. Crut, S. Shuman, M.-A. Bjornsti, and N. H. Dekker, Cellular strategies for Regulating DNA supercoiling: A single-molecule perspective, Cell **142**, 519 (2010).

[2] T. C. Boles, J. H. White, and N. R. Cozzarelli, Structure of plectonemically supercoiled DNA, J. Mol. Biol. **213**, 931 (1990).

[3] J. F. Marko and E. D. Siggia, Statistical mechanics of supercoiled DNA, Phys. Rev. E **52**, 2912 (1995).

[4] C. J. Dorman and M. J. Dorman, DNA supercoiling is a fundamental regulatory principle in the control of bacterial gene expression, Biophys. Rev. **8**, 209 (2016).

[5] S. Martis B., R. Forquet, S. Reverchon, W. Nasser, and S. Meyer, DNA supercoiling: An ancestral regulator of gene expression in pathogenic bacteria? Comput. Struct. Biotechnol. J. **17**, 1047 (2019).

[6] C. P. Johnstone and K. E. Galloway, Supercoiling-mediated feedback rapidly couples and tunes transcription, Cell Rep. **41**, 111492 (2022).

[7] H. P. Patel, S. Coppola, W. Pomp, U. Aiello, I. Brouwer, D. Libri, and T. L. Lenstra, DNA supercoiling restricts the transcriptional bursting of neighboring eukaryotic genes, Mol. Cell **83**, 1573 (2023).

[8] S. Deng, R. A. Stein, and N. P. Higgins, Organization of supercoil domains and their reorganization by transcription, Mol. Microbiol. **57**, 1511 (2005).

[9] N. Gilbert and J. Allan, Supercoiling in DNA and chromatin, Curr. Opin. Genet. Dev. **25**, 15 (2014).

[10] S. Corless and N. Gilbert, Effects of DNA supercoiling on chromatin architecture, Biophys. Rev. **8**, 245 (2016).

[11] R. Blossey, *Chromatin: Structure, Dynamics, Regulation* (Chapman and Hall/CRC, New York, 2017).

[12] H. Schiessel, *Biophysics for Beginners: A Journey Through the Cell Nucleus* (Jenny Stanford Publishing, New York, 2021).

[13] M. S. Guo, R. Kawamura, M. L. Littlehale, J. F. Marko, and M. T. Laub, High-resolution, genome-wide mapping of positive supercoiling in chromosomes, eLife **10**, e67236 (2021).

[14] W. Vanderlinden, T. Brouns, P. U. Walker, P. J. Kolbeck, L. F. Milles, W. Ott, P. C. Nickels, Z. Debyser, and J. Lipfert, The free energy landscape of retroviral integration, Nat. Commun. **10**, 4738 (2019).

[15] Y. Yan, Y. Ding, F. Leng, D. Dunlap, and L. Finzi, Protein-mediated loops in supercoiled DNA create large topological domains, Nucleic Acids Res. **46**, 4417 (2018).

[16] Y. Yan, F. Leng, L. Finzi, and D. Dunlap, Protein-mediated looping of DNA under tension requires supercoiling, Nucleic Acids Res. **46**, 2370 (2018).
[17] Y. Yan, W. Xu, S. Kumar, A. Zhang, F. Leng, D. Dunlap, and L. Finzi, Negative DNA supercoiling makes protein-mediated looping deterministic and ergodic within the bacterial doubling time, Nucleic Acids Res. **49**, 11550 (2021).
[18] W. Vanderlinden, E. Skoruppa, P. Kolbeck, E. Carlon, and J. Lipfert, DNA fluctuations reveal the size and dynamics of topological domains, PNAS Nexus **1**, pgac268 (2022).
[19] Y. Liu, V. Bondarenko, A. Ninfa, and V. M. Studitsky, DNA supercoiling allows enhancer action over a large distance, Proc. Natl. Acad. Sci. USA **98**, 14883 (2001).
[20] F. Benedetti, J. Dorier, and A. Stasiak, Effects of supercoiling on enhancer–promoter contacts, Nucleic Acids Res. **42**, 10425 (2014).
[21] T. R. Strick, J. F. Allemand, D. Bensimon, A. Bensimon, and V. Croquette, The elasticity of a single supercoiled DNA molecule, Science **271**, 1835 (1996).
[22] S. Forth, C. Deufel, M. Y. Sheinin, B. Daniels, J. P. Sethna, and M. D. Wang, Abrupt buckling transition observed during the plectoneme formation of individual DNA molecules, Phys. Rev. Lett. **100**, 148301 (2008).
[23] H. Wada and R. R. Netz, Plectoneme creation reduces the rotational friction of a polymer, Europhys. Lett. **87**, 38001 (2009).
[24] S. Neukirch and J. F. Marko, Analytical description of extension, torque, and supercoiling radius of a stretched twisted DNA, Phys. Rev. Lett. **106**, 138104 (2011).
[25] M. van Loenhout, M. de Grunt, and C. Dekker, Dynamics of DNA supercoils, Science **338**, 94 (2012).
[26] A. Fathizadeh, H. Schiessel, and M. R. Ejtehadi, Molecular dynamics simulation of supercoiled DNA rings, Macromol. **48**, 164 (2015).
[27] T. Lepage, F. Képès, and I. Junier, Thermodynamics of long supercoiled molecules: Insights from highly efficient Monte Carlo simulations, Biophys. J. **109**, 135 (2015).
[28] G. Forte, M. Caraglio, D. Marenduzzo, and E. Orlandini, Plectoneme dynamics and statistics in braided polymers, Phys. Rev. E **99**, 052503 (2019).
[29] J.-C. Walter, T. Lepage, J. Dorignac, F. Geniet, A. Parmeggiani, J. Palmeri, J.-Y. Bouet, and I. Junier, Supercoiled DNA and non-equilibrium formation of protein complexes: A quantitative model of the nucleoprotein ParBS partition complex, PLoS Comput. Biol. **17**, e1008869 (2021).
[30] Y. A. Fosado, D. Michieletto, C. A. Brackley, and D. Marenduzzo, Nonequilibrium dynamics and action at a distance in transcriptionally driven DNA supercoiling, Proc. Natl. Acad. Sci. USA **118**, e1905215118 (2021).
[31] A. L. Pyne, A. Noy, K. H. Main, V. Velasco-Berrelleza, M. M. Piperakis, L. A. Mitchenall, F. M. Cugliandolo, J. G. Beton, C. E. Stevenson, B. W. Hoogenboom *et al.*, Base-pair resolution analysis of the effect of supercoiling on DNA flexibility and major groove recognition by triplex-forming oligonucleotides, Nat. Commun. **12**, 1053 (2021).
[32] E. Skoruppa and E. Carlon, Equilibrium fluctuations of DNA plectonemes, Phys. Rev. E **106**, 024412 (2022).
[33] G. D. Watson, E. W. Chan, M. C. Leake, and A. Noy, Structural interplay between DNA-shape protein recognition and supercoiling: the case of IHF, Comput. Struct. Biotechnol. J. **20**, 5264 (2022).
[34] I. Junier, E. Ghobadpour, O. Espeli, and R. Everaers, DNA supercoiling in bacteria: state of play and challenges from a viewpoint of physics based modeling, Front. Microbiol. **14**, 1192831 (2023).
[35] S. B. Smith, L. Finzi, and C. Bustamante, Direct mechanical measurements of the elasticity of single DNA molecules by using magnetic beads, Science **258**, 1122 (1992).
[36] F. Mosconi, J. F. Allemand, D. Bensimon, and V. Croquette, Measurement of the torque on a single stretched and twisted DNA using magnetic tweezers, Phys. Rev. Lett. **102**, 078301 (2009).
[37] J. Lipfert, J. W. J. Kerssemakers, T. Jager, and N. H. Dekker, Magnetic torque tweezers: Measuring torsional stiffness in DNA and RecA-DNA filaments, Nat. Methods **7**, 977 (2010).
[38] J. D. Moroz and P. Nelson, Entropic elasticity of twist-storing polymers, Macromol. **31**, 6333 (1998).
[39] J. F. Marko, Torque and dynamics of linking number relaxation in stretched supercoiled DNA, Phys. Rev. E **76**, 021926 (2007).
[40] J. F. Marko, Biophysics of protein-DNA interactions and chromosome organization, Physica A **418**, 126 (2015).
[41] J. W. Shepherd, S. Guilbaud, Z. Zhou, J. A. L. Howard, M. Burman, C. Schaefer, A. Kerrigan, C. Steele-King, A. Noy, and M. C. Leake, Correlating fluorescence microscopy, optical and magnetic tweezers to study single chiral biopolymers such as DNA, Nat. Commun. **15**, 2748 (2024).
[42] M. Y. Sheinin, S. Forth, J. F. Marko, and M. D. Wang, Underwound DNA under tension: Structure, elasticity, and sequence-dependent behaviors, Phys. Rev. Lett. **107**, 108102 (2011).
[43] M. Emanuel, G. Lanzani, and H. Schiessel, Multiplectoneme phase of double-stranded DNA under torsion, Phys. Rev. E **88**, 022706 (2013).
[44] J. F. Marko and S. Neukirch, Competition between curls and plectonemes near the buckling transition of stretched supercoiled DNA, Phys. Rev. E **85**, 011908 (2012).
[45] X. Gao, Y. Hong, F. Ye, J. T. Inman, and M. D. Wang, Torsional stiffness of extended and plectonemic DNA, Phys. Rev. Lett. **127**, 028101 (2021).
[46] J. D. Moroz and P. Nelson, Torsional directed walks, entropic elasticity, and DNA twist stiffness, Proc. Natl. Acad. Sci. USA **94**, 14418 (1997).
[47] V. V. Rybenkov, N. R. Cozzarelli, and A. V. Vologodskii, Probability of DNA knotting and the effective diameter of the DNA double helix, Proc. Natl. Acad. Sci. USA **90**, 5307 (1993).
[48] B. A. Krajina and A. J. Spakowitz, Large-scale conformational transitions in supercoiled DNA revealed by coarse-grained simulation, Biophys. J. **111**, 1339 (2016).
[49] F. B. Fuller, The Writhing number of a space curve, Proc. Natl. Acad. Sci. USA **68**, 815 (1971).
[50] K. Klenin and J. Langowski, Computation of writhe in modeling of supercoiled DNA, Biopolymers **54**, 307 (2000).
[51] F. C. Oberstrass, L. E. Fernandes, and Z. Bryant, Torque measurements reveal sequence-specific cooperative transitions in supercoiled DNA, Proc. Natl. Acad. Sci. USA **109**, 6106 (2012).

[52] H. Brutzer, N. Luzzietti, D. Klaue, and R. Seidel, Energetics at the DNA supercoiling transition, Biophys. J. **98**, 1267 (2010).

[53] J. F. Marko and E. D. Siggia, Stretching DNA, Macromol. **28**, 8759 (1995).

[54] J. Ubbink and T. Odijk, Electrostatic-undulatory theory of plectonemically supercoiled DNA, Biophys. J. **76**, 2502 (1999).

[55] K. Dill and S. Bromberg, *Molecular Driving Forces: Statistical Thermodynamics in Biology, Chemistry, Physics, and Nanoscience* (Garland Science, New York, 2010).

[56] X. Viader-Godoy, C. R. Pulido, B. Ibarra, M. Manosas, and F. Ritort, Cooperativity-dependent folding of single-stranded DNA, Phys. Rev. X **11**, 031037 (2021).